Experimental Thermal and Fluid Science 109 (2019) 109891

Contents lists available at ScienceDirect

Experimental Thermal and Fluid Science

journal homepage: www.elsevier.com/locate/etfs

Single-phase forced convection heat transfer and pressure drop in circular tubes in the laminar and transitional flow regimes

A.I. Bashir[a], M. Everts[a], R. Bennacer[a,b,c], J.P. Meyer[a,*]

[a] Department of Mechanical and Aeronautical Engineering, University of Pretoria, Pretoria 0002, South Africa
[b] LMT, ENS-Cachan, CNRS, Université Paris Saclay, Cachan, France
[c] ECAM EPMI, 13 Blvd Hautil, F-95092, France

ARTICLE INFO

Keywords:
Forced convection
Fluid property
Transition
Laminar
Constant heat flux
Vertical
Upward
Downward

ABSTRACT

Forced convection experiments are challenging to perform in smooth horizontal circular tubes, because very low heat fluxes are required to ensure that the buoyancy effects do not enhance the heat transfer coefficients. Previous work in the transitional flow regime mainly focused on mixed convection and limited work has been conducted for forced convection heat transfer. It was therefore the purpose of this study to experimentally investigate the heat transfer and pressure drop characteristics during specifically forced convection conditions. Vertical upward and downward flows through a smooth circular test section were considered. Experiments were conducted using water (Prandtl numbers between 3.5 and 8.1) at Reynolds numbers of 400–6000 with constant heat fluxes varying from 1 to 8 kW/m^2. Although the flow direction and heat flux had no influence in the laminar flow regime, it was found that the fully developed laminar forced convection Nusselt numbers were not constant at 4.36, but were a function of Reynolds number for Reynolds numbers higher than 1000. Therefore, a revised laminar Nusselt number correlation for smooth circular tubes was developed. The fully developed laminar forced convection friction factors were, as expected, equal to 64/*Re*. For both the heat transfer and pressure drop characteristics, transition occurred at the same mass flow rates for all the heat fluxes, including isothermal flow, but the critical Reynolds numbers increased with an increase in heat flux. The width of the transitional flow regime in the fully developed region remained constant for all heat fluxes.

1. Introduction

For laminar convective flow through a tube, the flow can be either forced convection or mixed convection. With mixed convection, the density differences in the radial direction lead to buoyancy effects in the fluid. To be able to distinguish between forced convection and mixed convection is very important, because the Nusselt numbers of the different conditions vary significantly. Everts and Meyer [1] developed flow regime maps that can be used to determine whether forced or mixed convection conditions exist in horizontal tubes with a constant heat flux boundary condition. For vertical flow, Metais and Eckert [2] developed a flow regime map for both constant heat flux and constant surface temperature boundary conditions.

For forced convection heat transfer in circular tubes, most heat transfer textbooks [3–8] reported that for a constant heat flux boundary condition, the fully developed laminar Nusselt number is constant at 4.36, and independent of Reynolds number or Prandtl number. This Nusselt number of 4.36 was derived analytically, assuming constant fluid properties (density, viscosity, thermal conductivity and specific heat). However, for mixed convection conditions, the Nusselt numbers are easily 180–520% higher than 4.36 [9–11].

Metais and Eckert [2] considered the flow as forced convection when the Nusselt numbers were within 10% of 4.36. Hallman [12] obtained a Nusselt number of 4.62 at a low Rayleigh number of approximately 25 for vertical upward flow in circular tube. Meyer and Everts [11] recently obtained forced convection conditions with an average laminar Nusselt number of approximately 4.75 at a low heat flux of about 1 kW/m^2 and a Reynolds number of 941. In general, it was concluded that it is very challenging to experimentally obtain forced convection heat transfer with Nusselt number of 4.36, especially at higher heat fluxes and higher Reynolds numbers in the laminar flow regime [11]. However, Sudo et al. [13] performed forced convection experiments in vertical narrow rectangular channels and found that the effect of buoyancy was negligible on the flow direction (upward and downward flow) for Reynolds number higher than 700. Meyer et al. [14] also found that forced convection conditions could be obtained at

* Corresponding author.
E-mail address: josua.meyer@up.ac.za (J.P. Meyer).

https://doi.org/10.1016/j.expthermflusci.2019.109891
Received 22 March 2019; Received in revised form 2 July 2019; Accepted 7 August 2019
Available online 07 August 2019

Nomenclature

A	arbitrary point in Fig. 9
B	arbitrary point in Fig. 9
b	bulk
C_p	specific heat at constant pressure
D	diameter
DAQ	data acquisition system
DC	direct current
eb	energy balance error
f	friction factor/function
FD	fully developed
g	gravitational acceleration/function
Gr	Grashof number
h	heat transfer coefficient
I	current
i	data point index
j	colburn j-factor
k	thermal conductivity
L	length
$\dot{m}$	mass flow rate
n	constant
Nu	Nusselt number
P	pressure
Pr	Prandtl number
PT	pressure tap
$\dot{Q}$	heat transfer rate
$\dot{q}$	heat flux
r	radius
R	thermal resistance
Re	Reynolds number
Ri	Richardson number
T	temperature/thermocouples
u	velocity in axial direction
V	velocity/voltage
x	distance from tube inlet

Special characters

β	coefficient of thermal expansion
μ	dynamic viscosity
ρ	density

Subscripts

avg	average
b	bulk/bottom
cor	correlation
cp	constant property
cr	critical
Cu	copper
e	exit
exp	experiment
f	fluid/friction factor
FC	Forced Convection
FD	Fully Developed
$grav$	gravity
i	inlet/inner/data point index
iw	inner wall
m	mean
o	outer
$offset$	offset at no flow conditions
ow	outer wall
ΔP	pressure drop
qt	quasi-turbulent
t	thermal/top
vp	variable property
w	wall

a relatively high heat flux of 8 kW/m^2 for both upward and downward vertical flows.

Although the derivation of the Nusselt number of 4.36 during forced convection conditions was obtained for a constant heat flux boundary condition and constant properties, this is not the case in actual practice. The fluid properties change with temperature along the tube length. However, the properties can also change because of changes in mass flow rates and/or heat flux. Due to the challenge of conducting forced convection experiments, especially in the laminar flow regime, several numerical analyses focused on the effects of changes in fluid properties on the forced convection heat transfer and pressure drop characteristics in smooth tubes [15].

Nonino et al. [16] performed a numerical analysis on laminar forced convection developing flow for different horizontal channels including a circular tube with a constant wall temperature boundary condition. It was found that the change in viscosity with temperature along the channel length significantly affected the laminar forced convection heat transfer coefficients, while the other fluid properties were assumed to be constant. This is similar to the findings of Nouar [17] that the heat transfer coefficients were affected by a decrease in viscosity due to an increase in temperature along the tube length. Zhai et al. [18] investigated the effect of axial conduction due to the change in fluid properties on the laminar forced convection heat transfer coefficients. It was found that varying fluid properties had a greater influence on the velocity profile in the entrance region, while the temperature profile was more affected in the fully developed region.

Equations such as Eq. (1) [15] can therefore be used to account for changes in the fluid properties:

$$\frac{Nu_{vp}}{Nu_{cp}} = \left(\frac{\mu_b}{\mu_w}\right)^n \tag{1}$$

The variable property Nusselt number, Nu_{vp}, in Eq. (1) is a function of the constant property Nusselt number, $Nu_{cp} = 4.36$, viscosity ratio, (μ_b/μ_w), and n. Depending on the heating or cooling conditions with liquids or gases, different values of n were obtained based on regression analysis of some experimental data. For laminar fully developed flow with heating, Deissler [19] and Shannon and Depew [20] recommended $n = 0.14$ for liquids. From Eq. (1), it followed that the variable property Nusselt number, Nu_{vp}, increased with increasing heat flux due to the increase in viscosity ratio.

Herwig [21] numerically investigated the effect of different fluid properties, other than viscosity only, to correct the constant property Nusselt number. Eq. (2) is a more sophisticated equation that takes into consideration more fluid properties:

$$\frac{Nu_{vp}}{Nu_{cp}} = \left(\frac{\mu_w}{\mu_b}\right)^{-0.107}\left(\frac{\rho_w}{\rho_b}\right)^{0.34-\frac{0.128}{Pr}}\left(\frac{k_w}{k_b}\right)^{0.245}\left(\frac{c_{pw}}{c_{pb}}\right)^{0.255} \tag{2}$$

Eq. (2) shows the variable property Nusselt number, Nu_{vp}, as a function of the constant property Nusselt number, Nu_{cp}, and the ratios of viscosity, density, thermal conductivity and specific heat at the wall and bulk temperatures, respectively. Hence, Eq. (2) also followed a similar pattern than Eq. (1), where the Nusselt numbers increased with heat flux due to the increasing viscosity ratio, (μ_b/μ_w). A similar approach was also followed by Koppel and Smith [22].

Zhao et al. [23] recently developed a new correlation for the variable property Nusselt number, Nu_{vp}, numerically, with properties evaluated at the bulk fluid temperatures. This was to account for

property-temperature sensitivities, especially at higher bulk fluid temperatures, and for different fluids. However, because the correlation was a function of heat flux, the Nusselt numbers changed with heat flux. This is not necessarily the case for pure forced convection, as will be shown in this paper.

The effects of variable fluid properties on the forced convection heat transfer coefficients were also investigated by many researchers for micro-convective applications [24–26]. It was found that the effect of fluid properties on the forced convection heat transfer coefficients were significant. However, there is little experimental data available to validate and investigate the effects of the fluid properties, not only on laminar flow, but also on transitional flow forced convection heat transfer and pressure drop characteristics.

Literature indicates that the analyses of the heat transfer and pressure drop characteristics in the transitional flow regime for a constant heat flux boundary condition were generally conducted within horizontal tubes [10,11,14,27–36]. Furthermore, mixed convection was the dominating mode of heat transfer. Everts and Meyer [10] found that buoyancy effects significantly influenced both the start and end of the transitional flow regime and developed correlations for the boundaries of transitional flow regime for mixed convection heat transfer in horizontal tubes as a function axial location and buoyancy (Grashof number). However, for forced convection heat transfer, buoyancy effects are negligible (zero Grashof number condition) and this might change the behavior and boundaries of the transitional flow regime. Wei [37] recently identified six different flow and heat transfer regimes for laminar to turbulent forced convection flow in a smooth horizontal plane-channel. It was concluded that with the assumptions of no buoyancy or entrance effects, it was difficult to analytically predict the transition heat transfer coefficients from the governing equations.

Most of the transitional flow regime work in vertical tubes in literature were for either natural or mixed convection. Huber and Walter [38] studied forced convection heat transfer in the transition region of a co-current flow vertical heat exchanger between Reynolds numbers of 4000 and 10 000. However, transition in tubes occurred much earlier than a Reynolds number of 4000 depending on the rate of heating and inlet geometry [10,27,39]. Therefore, they also considered part of the quasi-turbulent and turbulent flow regimes as the transition region. Galanis and Behzadmehr [40] reviewed mixed convection heat transfer in vertical ducts and reported that the increase in heating can cause transition to occur at Reynolds numbers lower than 2000 in vertical tubes. Scheele et al. [41] used dye to study the effect of natural convection on transition from laminar flow to a disturbed flow along the length of a vertical tube. It was found that for upward flow, the growth of small disturbances along the length of the tube caused an instability within the flow that led to transition, while for downward flow, transition occurred suddenly because of the flow separation at the wall. Behzadmehr et al. [42] showed buoyancy effects caused an instability in the flow that led to the start of transition at different Reynolds numbers in vertical tubes. Their transition work concentrated on the start of transition along the tube length at low Reynolds numbers of 1000, 1300 and 1600 only, not the entire transitional flow regime. Hence, there is very limited information available for forced convection transitional flow in vertical tubes.

Under normal circumstances, fully developed forced convection conditions in the laminar and transitional flow regimes with a constant heat flux boundary condition are challenging to obtain experimentally. Although it is possible to obtain it in zero gravity conditions, small diameter tubes and by using small heat fluxes, the uncertainties are usually high due to the small temperature differences between the wall and fluid. However, it is vital for our fundamental understanding of internal forced convection heat transfer that accurate experimental results with low uncertainties are available in literature. It is therefore the purpose of this paper to experimentally determine the Nusselt numbers and friction factors for fully developed forced convection conditions, not only in the laminar flow regime, but also in the transitional flow regime. This paper contradicts (by making use of experimental measurements) the classical heat transfer theory for forced convection conditions in a circular tube for laminar fully developed flow with a constant heat flux boundary condition, that the Nusselt number is 4.36 for all Reynolds numbers and Prandtl numbers. It will be shown that this is correct only for Reynolds numbers between approximately 600 and 1000. At higher Reynolds numbers, the Nusselt numbers increased with increasing Reynolds number by approximately 26% up to the critical Reynolds number. However, we confirmed that the friction factors for fully developed forced convection laminar flows were indeed $64/Re$ (even for diabatic conditions with variable fluid properties).

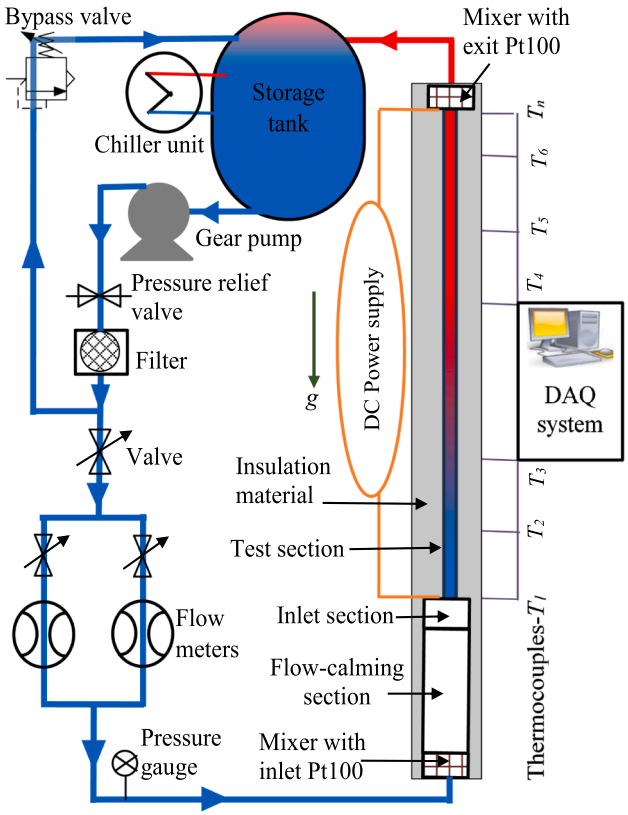

Fig. 1. Schematic layout of the experimental facility.

2. Experimental set-up

The complete experimental set-up (Fig. 1) has been described in detail by Meyer et al. [14] and is therefore only succinctly described in this paper. It comprises of a closed fluid loop, flow-calming section, inlet section, test section and the test bench structure. The test bench structure allowed that the inclination angle of the test section could be varied. Meyer et al. [14] found that forced convection conditions were obtained with the test section in a vertical orientation as shown schematically in Fig. 1.

Water was circulated from a 500 ℓ storage tank through flow meters, a flow-calming section and test section, and then back to the storage tank for cooling and recirculation. A chiller unit was coupled to the storage tank to cool down the heated water and maintain the water at a constant temperature.

A 420 ℓ/h magnetic gear pump was used to circulate the water through the test section. The pump was connected to the experimental set-up using a rubber hose to prevent any vibrations transmitted from the pump to the test section. The pump was controlled from a personal computer and the flow rate was changed by adjusting the voltage signal

sent through a Labview program.

A pressure relief valve was used to bypass the water back to the storage tank when the pressure exceeded the system pressure threshold value. A water bypass line was used to increase the backpressure in order to avoid flow pulsations in the test section that might influence the transitional flow inside the test section [43].

The mass flow rate of the water to the test section was measured using two Coriolis flow meters with different capacities. These flow meters had an accuracy of ± 0.05% of the full scale and a maximum flow rate of 330 ℓ/h and 108 ℓ/h, respectively. The flow meter with a higher flow rate (330 ℓ/h) was used for measurements in the quasi-turbulent and turbulent flow regimes, while the smaller flow meter (108 ℓ/h) was used for measurements in the laminar to quasi-turbulent flow regimes.

The mixer design of Bakker et al. [44] with alternating right and left hand twisted helical plates, was used for both the inlet and exit mixers. The inlet Pt100 probe was installed inside a soft Nylon mesh downstream of the inlet mixer. The outlet Pt100 probe was also installed just downstream of the outlet mixer with the water flowing along the probe in an axial direction [45].

2.1. Flow-calming section and inlet section

A flow-calming section was installed prior to the test section, as shown in Fig. 1, to ensure a uniform velocity distribution to the test section. A similar design to Ghajar and Tam [27] and Tam *et al.* [46] was used. However, the contraction ratio (ratio of the inner diameter of the flow-calming section to the inner diameter of the test section) was 33, while Ghajar and Tam [27] used a contraction ratio of 10. The flow-calming section consisted of a clear acrylic tube with an outer diameter and length of 180 mm and 616 mm, respectively, and three air bleed valves were located at the top of the tube to remove any trapped air.

Attached to the flow-calming section was the inlet section (containing a square-edged inlet), to ensure an undisturbed flow before entering the test section. It consisted of acrylic tube with a length of 235 mm and outer diameter of 180 mm. Special attention was given to ensure that the geometry of the inlet was a square-edged inlet, because Bashir et al. [39] has shown that the geometry of the inlet has a significant effect on the transition characteristics.

2.2. Test section

Fig. 2 is a schematic representation of the test section, indicating the two pressure tap locations, thermocouple stations, as well as the orientations for the upward and downward vertical flows. The test section was made from a smooth hard drawn copper tube with inner and outer diameters of 5.1 mm and 6.3 mm, respectively. The test section had a total length of 4.6 m and therefore a maximum length-to-diameter ratio (x/D_i) of 886. This length-to-diameter is much longer than that used previously in literature as discussed in Meyer and Everts [11].

The wall temperatures were measured at 21 thermocouple stations. T-type thermocouples with wire diameters of 0.25 mm were soldered to the outer surface of the tube. As shown in Fig. 2, the thermocouple stations were located at closer intervals near the entrance and in the fully developed part to capture enough data in these regions. Due to the small diameter of the test section, three thermocouples were used at each station. One thermocouple at the top (0°) and bottom (180°) of the tube and another thermocouple alternating at the sides between 90° (for station 1, 3, 5, etc.) and 270° (for station 2, 4, 6, etc.).

The theoretical thermal entrance length, L_t, for forced convection was calculated to be 3.2 m (based on $L_t = 0.05 RePrD_i$ for a Reynolds number of 2100 and a Prandtl number of 6). Therefore, conservatively the last 1.4 m of the test section always had fully developed flow and was considered as the "fully developed" region of the test section. The pressure drop and heat transfer measurements for the fully developed results were therefore taken in this region. Two pressure tap stations (PT-1 and PT-2 with length $L_{\Delta p}$ shown in Fig. 2) were located 1 m apart within the fully developed region and corresponded closely to the last six temperature-measuring stations, which were 1.05 m apart.

To ensure that the pressure taps did not cause any flow obstructions within the test section, a 0.5 mm diameter hole was drilled through each pressure tap. This hole was less than 10% of the inner diameter of

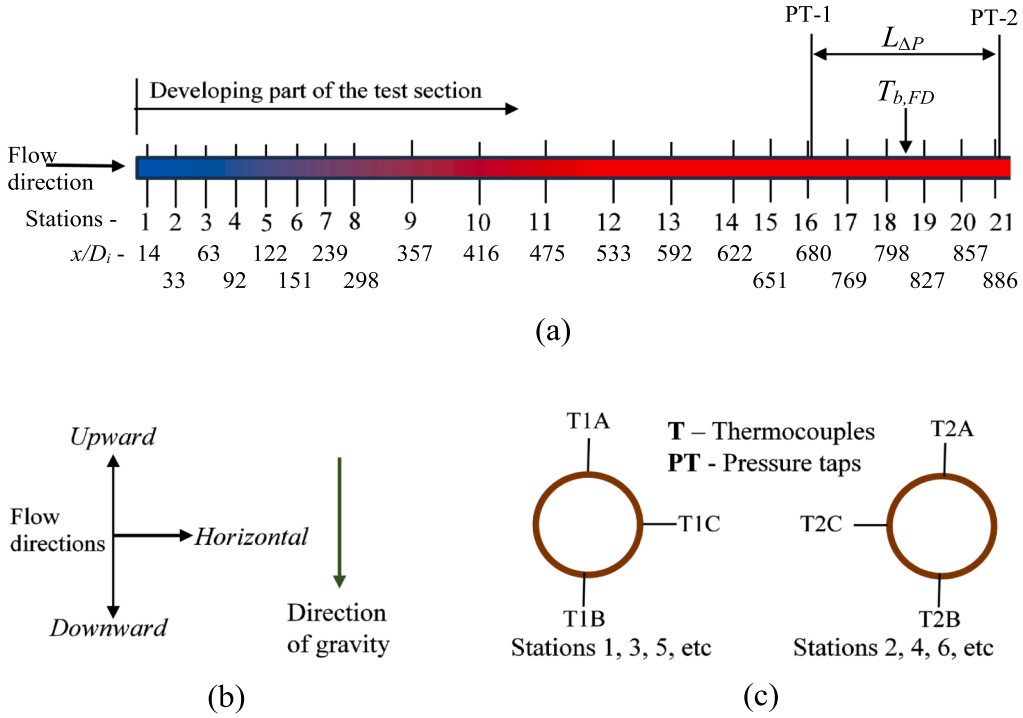

Fig. 2. Schematic representation of (a) the test section indicating the pressure taps and thermocouple stations, (b) the flow directions and (c) a cross section of the test section that shows the thermocouple positions per station.

the tube, as suggested by Rayle [47]. The holes were properly de-burred to avoid any local increase in pressure drop due to presence of burrs that might have formed during the drilling process. A differential pressure transducer with an interchangeable diaphragm was connected to the pressure taps using a Nylon tube. Two different diaphragms were used for the high and low pressure drop measurements. The ranges and accuracies of all the instruments used are given in Table 1.

For a constant heat flux boundary condition, two T-type constantan heating wires, with diameters of 0.38 mm, were tightly coiled around the test section (skipping the thermocouple junctions) and connected in parallel to a DC power supply. The two heating wires were connected in opposite polarities to avoid electromagnetic interferences due to the applied currents [43].

2.3. Test bench

A 6 m long test bench was built to accommodate the test section with the flow-calming section. The test bench was placed on a rigid frame with a height of 3 m and damping pads were used to avoid possible vibrations from the floor and equipment to the test section. The test bench was pivoted at the center such that it could be fixed at vertically upward and vertically downward directions. Tension cables were used keep the test bench straight and rigid. A digital inclinometer was attached to the test bench and used to verify the test section inclination angle (vertical upward and vertical downward orientations).

2.4. Insulation

The flow-calming section, inlet section, test section, mixers and tubes were insulated using insulation material with a thermal conductivity of 0.034 W/(mK) to prevent heat transfer to the environment,. The thickness of the insulation around the test section was 60 mm and the maximum heat loss was estimated with one-dimensional heat transfer calculations (taking into consideration the average measured wall and outside insulation temperatures and insulation resistance) to be less than 2%.

2.5. Experimental procedure

Steady-state conditions were reached two hours after the first start-up of a day. Steady-state conditions were assumed once there were no significant changes in the mass flow rates, temperatures, currents, pressure drops and energy balance readings. Experiments were conducted by starting with the highest mass flow rate and then decreasing the mass flow rates by adjusting the pump speed in a Labview program. To minimize flow pulsations, the bypass and supply valves were continuously adjusted such that the pump could operate at higher mass flow rates. The heat fluxes were produced by a DC power supply by applying the required voltages and currents.

Measurements were taken at greater mass flow rate intervals in the laminar and turbulent flow regimes, but at closer intervals near and within the transitional flow regime. After each Reynolds number increment, approximately 5–10 min in the quasi-turbulent and turbulent flow regimes and 15–20 min in the laminar flow regime, were required to reach steady-state conditions. In the transitional flow regime, fluctuations in temperature, mass flow rate, pressure drop, and energy balance were observed, therefore more time (approximately 20–30 min) was required to reach steady-state. Once steady-state was achieved, 400 data points were logged at a frequency of 20 Hz. These data points were then averaged to obtain one data point. The data logged included the inlet and exit temperatures, wall temperatures, ambient temperatures, mass flow rates and pressure drops. The temperature of the water in the storage tank was also monitored to ensure a constant inlet temperature to the test section. This procedure was used for the test section in vertical upward and downward flow orientations, as well as limited experiments in a horizontal orientation for validation purposes. All the data obtained were saved and used in a separate program for the analysis.

2.6. Experimental test matrix

Table 2 summarizes the matrix of experiments captured at various heat fluxes from isothermal (0 kW/m^2) to 8 kW/m^2. A total of 385 mass flow rate measurements, 25,025 temperature measurements and 385 pressure drop measurements were obtained. Experimental results from Meyer et al. [14] for mixed convection conditions for horizontal flow were used for a part of this study for comparison purposes. It should be noted that the database (summarized in Table 2) collected for this study is approximately one order of magnitude larger than that of previous studies for (vertical tubes) that varied from 2633 [48] to 4200 [49] temperature measurements, 5 [50] – 44 [51] pressure drop measurements and 2 [52] – 56 [49] mass flow rate measurements. It can therefore be expected that with our large data base, it will be possible to generate much more phenomena than what was identified previously.

3. Data reduction

Over the tube with measured length, L, the fluid temperatures, $T(x)$, at any axial position, x, were determined from the measured inlet, T_i, and exit, T_e, average fluid temperatures as obtained from the two Pt100 probes located at the tube inlet and tube outlet:

$$T(x) = T_i + \frac{(T_e - T_i)}{L}x \tag{3}$$

Linear temperature profiles were assumed for the temperatures, because constant heat fluxes were applied to the test section. The bulk temperature for the fully developed part of the test section, ($T_{b,FD}$ in Fig. 2), could therefore be determined at the measured distance $x = 3.92$ m from the inlet as shown in Fig. 2(a). Depending on what was required (fully developed bulk values or local values) these temperatures were also used to determine all the fluid properties (densities, ρ, viscosities, μ, thermal conductivities, k, specific heat, C_p, and Prandtl numbers, Pr) using the correlations of Popiel and Wojtkowiak [53] for water.

The single-phase pressure drops were estimated using a similar approach than references [51,54–59]. The frictional pressure drops, ΔP_f, used to calculate the friction factors were obtained from Eq. (4):

$$\Delta P_f = \Delta P_{exp} - \Delta P_{grav} \tag{4}$$

ΔP_{exp}, were the measured pressure drops, $\Delta P_{measured}$, obtained from the differential pressure transducers and were corrected by the pressure offset, ΔP_{offset}, at no flow conditions. This accounted for the vertical height ($L_{\Delta p}$ in Fig. 2) pressure difference between the pressure taps at isothermal conditions:

$$\Delta P_{exp} = \Delta P_{measured} + \Delta P_{offset} \tag{5}$$

When heat was applied, the gravitational pressure drops, ΔP_{grav} in Eq. (4), were due to the density difference with and without heating (due to temperature gradients) and were defined as the pressure

Table 1
Ranges and accuracies of the instrumentation used.

Instruments	Range	Accuracy
DC power supply	0–1 500 W	3 W
Inclinometer	0–360°	0.2°
Pt100 probes	0–100 °C	0.06 °C
Thermocouples	−200 to 350 °C	0.1 °C
Pressure transducers	0–3.5 kPa	8.75 Pa
	0–14 kPa	35 Pa
Coriolis flow meters		
CMFS010	0–108 ℓ/h	0.054 ℓ/h
CMFS015	0–330 ℓ/h	0.165 ℓ/h

Table 2
Experimental test matrix.

Tube orientation	Heat flux [kW/m^2]	Reynolds number range	Mass flow rate measurements	Temperature measurements	Pressure drop measurements
Vertical upward	0	600–6000	40	2600	40
	1	250–2922	37	2405	37
	2	375–2049	19	1235	19
	4	1086–5892	38	2470	38
	6	1571–5778	36	2340	36
	8	2153–5985	36	2340	36
Vertical downward	0	600–6000	40	2600	40
	1	453–1508	14	910	14
	2	337–2052	18	1170	18
	4	1092–6097	37	2405	37
	6	1576–5874	37	2405	37
	8	2150–5887	33	2145	33
Total			385	25,025	385

difference between the pressure at the reference inlet fluid temperature before heating (isothermal) and the average pressure within the heated test section (between the pressure taps):

$$\Delta P_{grav} = \rho_{b,FD} g L_{\Delta P} - \rho_i g L_{\Delta P} = (\rho_{b,FD} - \rho_i) g L_{\Delta P} \tag{6}$$

where $\rho_{b,FD}$ and ρ_i were the bulk density obtained from the temperature at the bulk fully developed station in Fig. 2(a) and the density at the inlet (before the fluid is heated in the test section), respectively. The gravitational acceleration, g, was taken as 9.81 m/s^2 and $L_{\Delta P}$ was the measured distance between the two pressure taps.

The friction factors, f, were obtained from the calculated frictional pressure drops, ΔP_f, as follows:

$$f = \frac{2\Delta P_f}{\rho_{b,FD} V_{avg}^2} \frac{D_i}{L_{\Delta P}} = \frac{\Delta P_f \rho_{b,FD} \pi^2 D_i^5}{\dot{m}^2 8 L_{\Delta P}} \tag{7}$$

The measured tube inner diameter, D_i, was 5.1 mm, the measured distance, $L_{\Delta p}$, between the two pressure taps was 1 m, and the mass flow rates, $\dot{m}$, were obtained from the measured Coriolis flow measurements.

The local or bulk fully developed Reynolds numbers were calculated from the measured mass flow rates:

$$Re = \frac{4\dot{m}}{\pi D_i \mu} \tag{8}$$

with the viscosities, μ, determined at the local mean fluid temperature, $T(x)$, or at the bulk fully developed temperature, '*b,FD*' station as shown in Fig. 2.

The effective heat transfer rates, $\dot{Q}_f$, to the fluid were determined from the measured mass flow rates, $\dot{m}$, and the difference between the measured inlet and exit fluid temperatures:

$$\dot{Q}_f = \dot{m} C_p (T_e - T_i) \tag{9}$$

The energy balance error, *eb*, was used to compare the measured heat transfer to the water, $\dot{Q}_f$, with the electrical energy supplied, $\dot{Q} = I \times \Delta V$, and is given as:

$$eb = \left[\frac{\dot{Q} - \dot{Q}_f}{\dot{Q}} \right] \times 100 \tag{10}$$

where I and ΔV were the measured currents and voltage drops, respectively.

The heat flux applied to the fluid, $\dot{q}_f$, was calculated as follows:

$$\dot{q}_f = \frac{\dot{Q}_f}{\pi D_i L} \tag{11}$$

The heat transfer rate to the fluid, $\dot{Q}_f$, was used to determine the heat flux rather than the electrical power supplied, $\dot{Q}$, because the electrical power supplied was always a little larger than the heat transfer rate to the water, $\dot{Q}_f$, because of the heat losses from the test section. These heat losses were on average 2.5% and corresponded well to the theoretical determined heat losses taking into consideration the resistance of the insulation material, the average measured wall temperatures and the measured temperatures on the outside of the insulation wall.

The local heat transfer coefficients at any axial point, x, from the tube inlet were determined as:

$$h = \frac{\dot{q}_f}{T_{iw} - T(x)} \tag{12}$$

where $T(x)$ was obtained from Eq. (3) and T_{iw} was the inner wall temperature obtained by taking into consideration the tube thermal resistance, R_w, in Eq. (13) as:

$$T_{iw} = T_{ow} - \dot{Q}_f R_w \tag{13}$$

The outside wall temperatures, T_{ow}, were the average of the three thermocouple measurements at each station. The tube conductive thermal resistance, R_w, was determined from Eq. (14) as:

$$R_w = \frac{ln(D_o/D_i)}{2\pi k_w L} \tag{14}$$

where D_o (6.3 mm) and D_i (5.1 mm) were the measured tube outer and inner diameters, respectively, and k_w was the thermal conductivity of the copper tube which was 401 W/(m K) [3].

These calculations showed that the temperature differences between the inside and outside walls were negligible and much smaller than the uncertainties of the thermocouple measurements. Although these differences were taken into consideration in this study, for all practical purposes it could be assumed that the inner wall temperatures were equal to the measured outside wall temperatures.

From the local heat transfer coefficients, the local Nusselt numbers were calculated as:

$$Nu = \frac{hD_i}{k} \tag{15}$$

The average Nusselt numbers of the fully developed part of the test section from x = 3.47 m (station 16 in Fig. 2) to x = 4.52 m (station 21) were taken as the average of the local Nusselt numbers at the last six measuring stations.

Also determined were the Colburn j-factors in Eq. (16):

$$j = \frac{Nu}{RePr^{\frac{1}{3}}} \tag{16}$$

and the Grashof numbers, Gr, based on the diameter as the characteristic length:

$$Gr = \frac{g\beta\rho^2 (T_w - T(x)) D_i^3}{\mu^2} \tag{17}$$

The average values of the Grashof numbers over the fully developed part of the test section were determined by averaging the last six values.

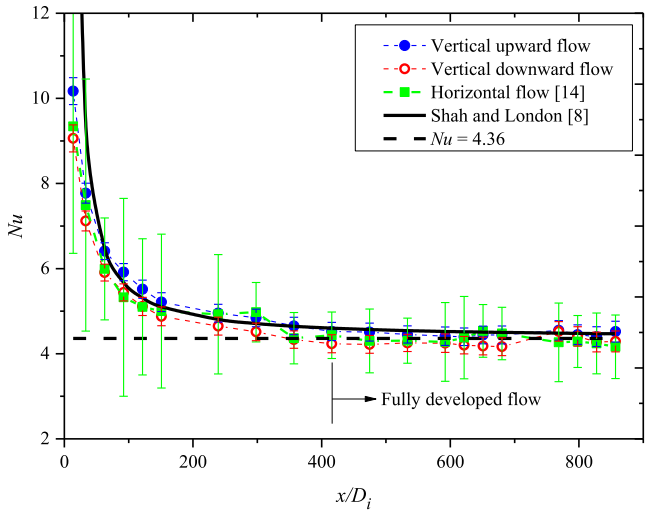

Fig. 3. Comparison of local Nusselt numbers as a function of axial location for vertical and horizontal flow orientations. The horizontal tube is at a bulk Reynolds number of 660 and a very low heat flux of 280 W/m^2 [14]. The flows for vertical upward and vertical downward orientations are at a bulk Reynolds number of approximately 1050 and a high heat flux of 4 kW/m^2.

The width of the transitional flow regime, ΔRe, as recently defined by Everts and Meyer [10], was calculated using the Reynolds numbers at the start, Re_{cr}, and end, Re_{qt}, of the transitional flow regime:

$$\Delta Re = Re_{qt} - Re_{cr} \tag{18}$$

Re_{cr}, was obtained as [10]:

$$Re = Re_{cr} \quad \text{when:} \left(\frac{dj}{dRe}\right)_{i-2:i} \approx 0 \tag{19}$$

where i-2:i means that at any given point i, dj/dRe was determined from the three data points at $Re(i\text{-}2)$, $Re(i\text{-}1)$ and $Re(i)$ for increasing Reynolds numbers. While Re_{qt}, was defined as [10]:

$$Re = Re_{qt} \quad \text{when:} \left(\frac{d^2Nu}{dRe^2}\right)_{i:i+2} \geq -0.00015 \tag{20}$$

where i:i + 2 means that at any given point i, the dNu/dRe was determined from the three data points at $Re(i)$, $Re(i + 1)$ and $Re(i + 2)$ for increasing Reynolds numbers (while Eq. (19) used the results at the previous two Reynolds numbers).

4. Uncertainties

All uncertainties were estimated within a 95% confidence level as prescribed by Dunn [60]. For the uncertainty analyses of this paper, the manufacturer instrumentation errors were used as the fixed errors and two times the standard deviation of 400 data points were used as the random errors. The thermocouples and Pt100 probes were calibrated against a reference thermometer with an accuracy of ± 0.03 °C. The maximum Reynolds number uncertainty was found to be approximately 1.8%. The maximum friction factor uncertainty in the laminar region was 8.5% and it reduced to approximately 2.3% in the turbulent flow regime. In the transitional flow regime, the friction factor uncertainty increased to a maximum of 14%. This was due to fluctuations of the mass flow rates, temperatures and pressure drop measurements within the transitional flow regime [10].

The maximum Nusselt number uncertainties were 3%, 13%, and 6%, respectively, in the laminar, transitional and turbulent flow regimes at the maximum heat flux of 8 kW/m^2. Again, the higher uncertainties in the transitional flow regime were caused by the higher fluctuations in the wall and exit temperature measurements. It has also been found that the vertical upward flow uncertainties were approximately the same than the vertical downward flow uncertainties and were both lower than the uncertainties in the horizontal flow orientation.

5. Validation

The heat transfer and pressure drop results were validated with the test section in horizontal and vertical orientations. The detailed validations of the experimental results for a horizontal orientation can be found in Meyer et al. [14] and a summary of the important conclusions are given with the vertical results in Sections 5.1 − 5.3. To ensure that forced convection conditions were achieved in the fully developed region of the test section, the start of the laminar fully developed region, as well as the effect of flow direction on the results were investigated.

5.1. Isothermal pressure drops

The laminar isothermal friction factors for horizontal flow compared well with the Poiseuille [61] correlation between Reynolds numbers of 600 and 2200 with an average deviation of 2.7% and a maximum deviation of 5%. In the turbulent flow regime, the experimental data compared well with the Blasius [62] correlation between Reynolds numbers of 4000 and 6000, with an average deviation of 1% and a maximum deviation of 1.7%. The results correlated very well for vertical flow as well. In the laminar flow regime, the average and maximum deviations were 2.9% and 5%, respectively, while in the turbulent flow regime, the deviations were 1% and 1.8%, respectively.

5.2. Laminar forced convection heat transfer

To verify the start of the fully developed region, Fig. 3 compares the horizontal forced convection local Nusselt numbers of Meyer et al. [14] at a Reynolds number of 660 and a very low heat flux of 280 W/m^2 (with a maximum uncertainty of 17% in the fully developed region), with the vertical upward and downward flow results. The vertical upward and downward results were at a bulk Reynolds number of 1050 and a high heat flux of 4 kW/m^2. The solid black line represents the forced convection correlation of Shah and London [8].

Fig. 3 shows that the Nusselt numbers for both vertical and horizontal orientations decreased along the tube length in the entrance region, as the thermal boundary layer developed, up to where the Nusselt numbers became relatively constant along the tube length from approximately $x/D_i = 416$, corresponding to the thermal entrance length. The flow was therefore fully developed from $x/D_i = 416$ for all the flow orientations in Fig. 3, where all the fully developed local Nusselt numbers were within 4.7% of the constant property Nusselt number of 4.36. The fully developed local Nusselt numbers for the vertical and horizontal flow orientations correlated very well with the correlation of Shah and London [8] with an average deviation of 4% and a maximum deviation of 8%.

To ensure that the flow in the fully developed region will always be fully developed, Fig. 4 compares the local Nusselt numbers along the axial location of the tube at a higher Reynolds number (close to the start of the transitional flow regime) and more heat fluxes than in Fig. 3, for both upward and downward flows. As expected, the Nusselt numbers decreased along the tube length and became relatively constant between $416 < x/D_i \leq 475$, indicating that the flow became fully developed. Therefore, Figs. 3 and 4 confirmed that for $x/D_i \geq 416$, the flow was fully developed for the horizontal, as well as the vertical upward and downward orientations. The last six thermocouple stations used for the fully developed analysis in this study were within $680 < x/D_i \leq 886$ (much longer than the thermal entrance).

Figs. 3 and 4 show that the Nusselt numbers for horizontal flows, as well as vertical upward and downward flows, were approximately the same. The maximum difference of 8% was found in the developing region at $x/D_i \approx 122$ at a heat flux of 4 kW/m^2 in Fig. 4. However, once

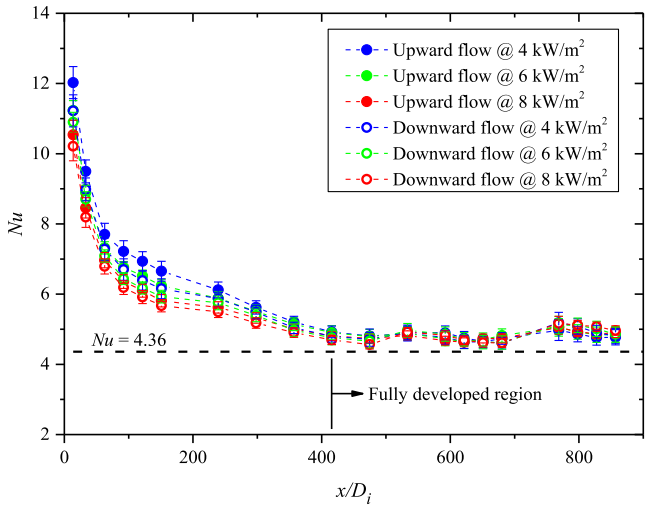

Fig. 4. Comparison of local Nusselt numbers as a function of axial location at higher heat fluxes and a Reynolds number of approximately 2100 for vertical upward and downward flows.

the flow was fully developed, the average and maximum differences were only 2% and 4%, respectively. Therefore, it was confirmed that tube orientation and flow direction had no influence on the laminar Nusselt numbers.

To investigate the effect of buoyancy on the wall temperatures, Fig. 5 compares the average wall temperature differences between the top and bottom of the test section, at the same heating condition, as a function of Reynolds number for vertical upward and horizontal [14] flows. This figure indicates that for horizontal flow at a heat flux of 6 kW/m^2, the minimum temperature difference was 0.12 °C, which was greater than the thermocouple uncertainty, thus indicating the presence of buoyancy effects that caused secondary flow and mixed convection. This temperature difference decreased with an increase in Reynolds number for horizontal flow.

However, for vertical upward flow, the corresponding wall temperature differences were approximately constant and were less than the uncertainty of the temperature measurements. This indicated the absence of buoyancy effects and hence confirmed forced convection heat transfer. This means that all the peripheral wall temperatures at a specific measuring station were approximately equal. Similar results were obtained with other heat fluxes and Reynolds numbers, as well as for downward flow. Because the upward and downward flow results were similar, it confirmed negligible buoyancy effects.

Furthermore, to confirm that forced convection conditions existed for all the fully developed local laminar heat transfer results of this study, the results were plotted on the flow regime map of Metais and Eckert [2] in Fig. 6. This flow regime map is valid for both vertical upward and downward flows in circular tubes with constant heat flux and constant wall temperature boundary conditions and for $0.01 < PrD_i/L < 1$. Fig. 6 show that all the results ($0.01 < PrD_i/L < 0.02$) of both upward and downward flows were within the laminar forced convection region. Again, confirming forced convection heat transfer for laminar vertical flow ($600 \le Re \le Re_{cr}$). Comparing the Richardson number, which is the ratio of buoyancy forces to viscous forces (Gr/Re^2), also confirmed forced convection conditions, because all the Richardson numbers were less than 0.1 ($0.0001 \le Ri \le 0.01$).

Although our experimental set-up was not developed for Reynolds numbers below approximately 300 (because of the range limitations of our Coriolis mass flow meters), limited experiments were conducted at lower Reynolds numbers. It was found from the heat transfer results that at Reynolds numbers of 400 and 600, assisting and opposing flows became significant and the Nusselt numbers decreased significantly.

5.3. Turbulent flow

For the turbulent heat transfer validation [14], the average Nusselt numbers (Fig. 7) were compared with the correlations of Gnielinski [64] and the newly developed and more accuate Meyer *et al.* [65]. The results of both horizontal and vertical flow correlated well with these correlations with average deviations of 6.1% and 5.6%, respectively, and maximum deviations of 13% and 8.6%, respectively. The deviations between the experimental results and literature were larger in the turbulent flow regime than in the laminar flow regime. This was expected because the temperature differences between the wall and fluid decreased with increasing Reynolds number, which led to increased uncertainties.

6. Results: laminar flow

The comparisons of the results were made based on Nusselt numbers, heat fluxes and Reynolds numbers for vertical upward and downward flows in the laminar and transitional flow regimes. Limited results with the flow in a horizontal orientation from Meyer *et al.* [14] were also included. The heat transfer characteristics of the entrance and fully developed regions as well as the fully developed pressure drop characteristics were analyzed. The general notation used in most graphs was solid circle markers (●) for upward flows and empty circle markers (○) for downward flows. It should be noted that the solid circle markers used in most graphs' legend were to differentiate the colors of the heat fluxes used for all the flow orientations. Furthermore, for clarification, only the vertical upward flow results were included in some of the graphs and not the downward results as well, because it was concluded from Figs. 3 and 4 that flow direction had no influence on the results.

6.1. Heat transfer

Fig. 8 compares the forced and mixed (obtained from Meyer et al. [14]) convection laminar Nusselt numbers for the same heating conditions but at different orientations. This figure indicates that for vertical flow, the average Nusselt numbers were approximately the same for all the heat fluxes (1–8 kW/m^2), indicating negligible or no buoyancy effects (Grashof numbers). However, for horizontal flow [14], the Nusselt numbers increased with increasing heat flux due to buoyancy effects, indicating mixed convection heat transfer.

The fully developed forced convection Nusselt numbers in Fig. 8 were not constant at 4.36, but increased slightly with increasing Reynolds numbers for all the heat fluxes. However, Fig. 4 confirmed that this increase was not due to entrance effects, because the flow was fully

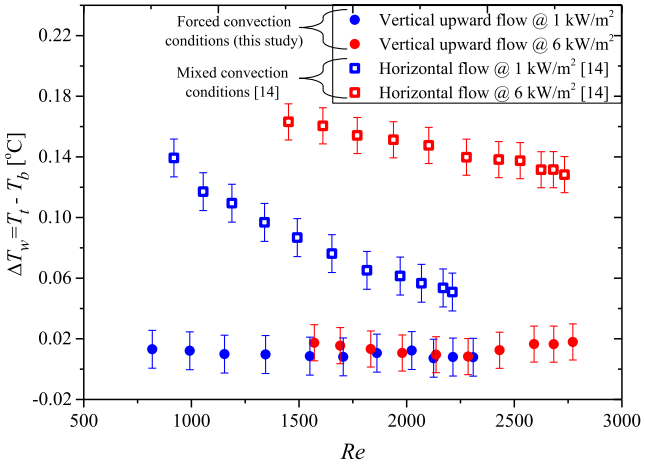

Fig. 5. Comparison of the average wall temperature difference between the top and bottom thermocouples for horizontal flow [14] and vertical upward flow as a function of Reynolds number at different heat fluxes.

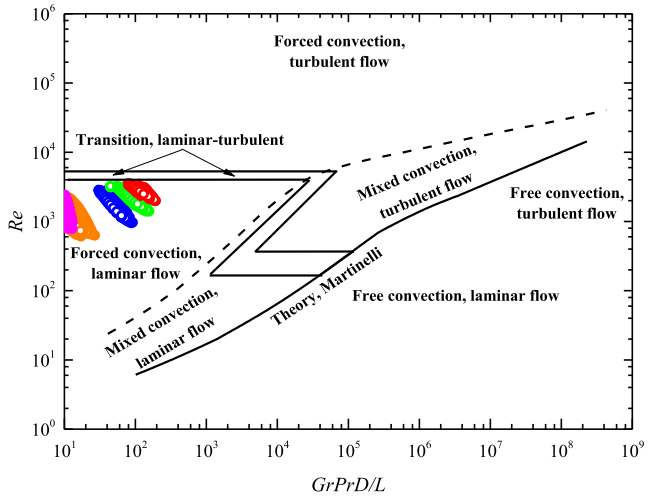

Fig. 6. Comparison of the laminar forced convection results on the flow regime map of Metais and Eckert [63] for heat fluxes of 1 kW/m^2 (pink), 2 kW/m^2 (orange), 4 kW/m^2 (blue), 6 kW/m^2 (green) and 8 kW/m^2 (red) for both vertical upward and downward flow at all the axial locations in the fully developed region ($416 < x/D_i < 857$). (For interpretation of the references to colour in this figure legend, the reader is referred to the web version of this article.)

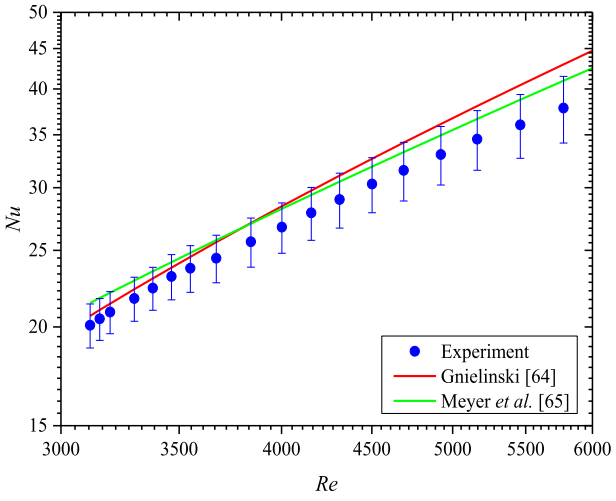

Fig. 7. Comparison of the average fully developed turbulent Nusselt numbers as a function of Reynolds number with literature.

developed from $x/D_i \geq 416$ at a Reynolds number of 2 100 and the Nusselt numbers in Fig. 8 were the average of $680 < x/D_i < 886$. This figure therefore indicates that the fully developed forced convection Nusselt numbers were a function of Reynolds number and were not constant at 4.36. Literature [15,17–24,26,66] reported that the deviation of the forced convection Nusselt numbers from the constant property Nusselt number of 4.36, were generally due to changes in fluid properties (the specific properties were normally not stated and/or the specific reasons were vague). The fluid properties changed with temperature either due to changes in heat flux or mass flow rate.

Fig. 9 contains a schematic representation of the changes in temperature, pressure drop, heat transfer coefficient, Reynolds number and viscosity along the tube length in both the entrance and fully developed regions. In the fully developed region, points A and B represent the bulk property/quantity as well as the pressure drop between points 1–2 and points 2–3, respectively. The maximum increase in fluid temperature (red line) between points A and B (1 m apart) occurred at a Reynolds number of 2153 (mass flow rate of 0.00474 kg/s) and a heat flux of 8 kW/m^2. For this case, the changes in fluid properties between the two

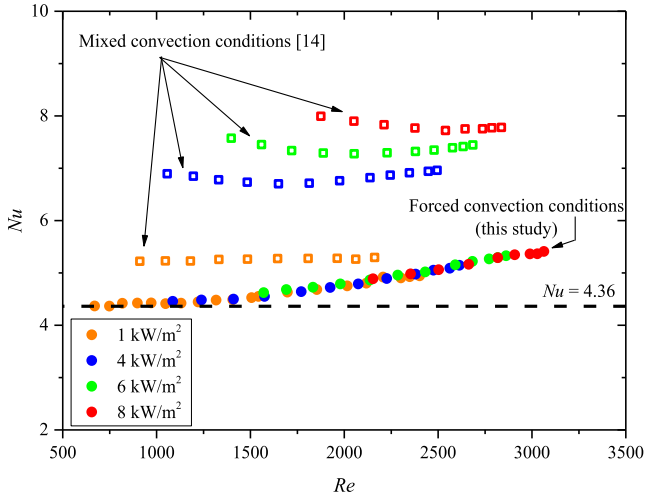

Fig. 8. Comparison of the average fully developed laminar Nusselt numbers as a function Reynolds number at various heat fluxes for vertical upward flow (forced convection heat transfer). Results for mixed convection horizontal flow (empty square markers) [14] were included for comparison at the same heating conditions.

points A and B were as follows: an increase in thermal conductivity and specific heat capacity of 0.8% and 0.04%, and a decrease in density, viscosity and Prandtl number of 0.3%, 13% and 12%, respectively. Thus, in general, the local changes in the fluid properties along the tube length were negligible, except for the changes in viscosity (blue line in Fig. 9) and thus Prandtl number, which were orders of magnitude more than for the other properties.

Because of the changes in viscosities (blue line), the local Reynolds number (green line) at position A ($Re_A = 1955$) increased with 13% to point B ($Re_B = 2193$). Furthermore, the decreasing viscosity also caused the pressure drops (calculated from Eq. (7)) to decrease with 10% from $\Delta P_A = 174$ Pa to $\Delta P_B = 156$ Pa. Therefore, dP/dx decreased in the axial direction and was not constant.

Fig. 10(a) compares the heat transfer coefficients as a function of mass flow rate for different heat fluxes. This figure indicates that for fixed mass flow rates of 0.002, 0.005 and 0.008 kg/s, an increase in heat flux from points 1 to 3 (brown), 4 to 8 (cyan) and 9 to 12 (black), respectively, led to increased heat transfer coefficients. Furthermore,

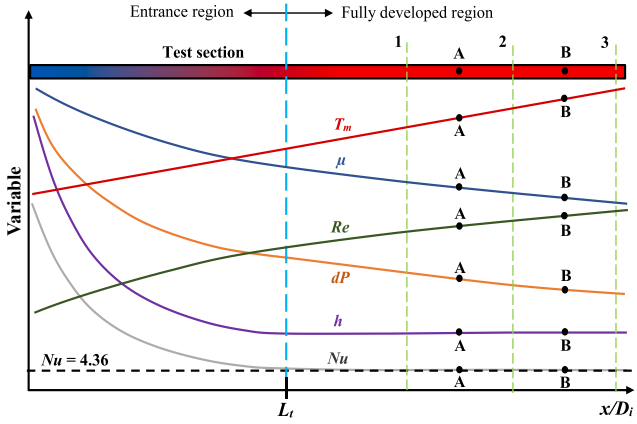

Fig. 9. Schematic representation of the variation of the mean fluid temperature, T_m, (red), viscosity, μ, (blue), Reynolds number, Re, (green), pressure drop, dP, (orange), heat transfer coefficient, h, (purple) and the Nusselt number, Nu, (grey) in the flow direction along the axial location of the test section tube for a contant heat flux boundary condition. (For interpretation of the references to colour in this figure legend, the reader is referred to the web version of this article.)

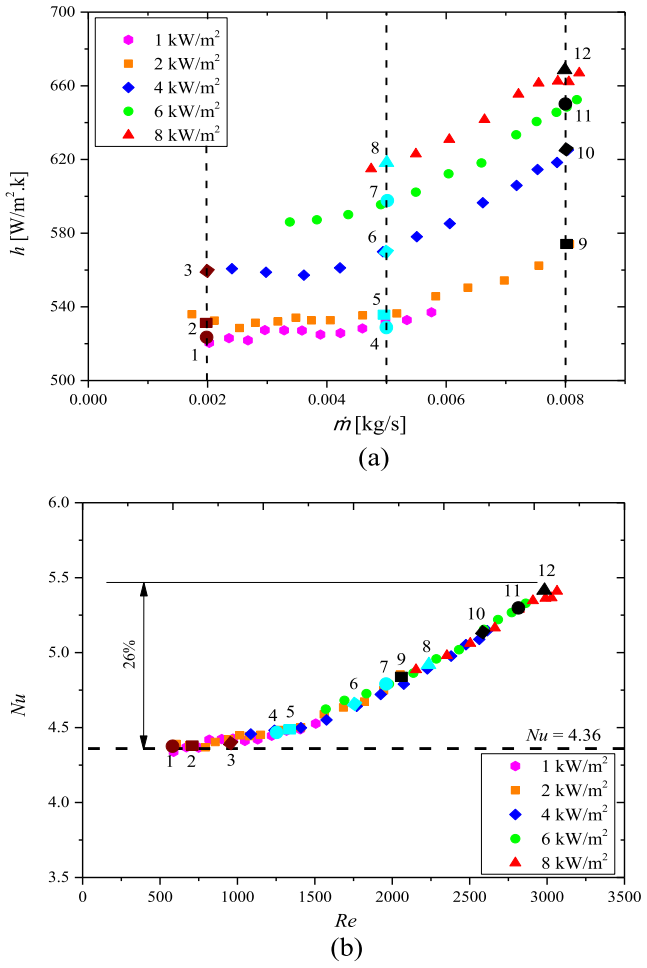

Fig. 10. Comparison for upward flow of (a) the heat transfer coefficients as a function mass flow rate and (b) the Nusselt numbers as a function of Reynolds number for different heat fluxes.

for mass flow rates greater than 0.003 kg/s, the heat transfer coefficients increased slightly with increasing mass flow rates.

To account for the changes in fluid properties, the heat transfer coefficients in Fig. 10(a) were plotted in terms of the non-dimensional Nusselt number as a function of Reynolds number (which is the non-dimensional mass flow rate) in Fig. 10(b). Points 1 to 12 in Fig. 10(a) correspond to the same points in Fig. 10(b). For a fixed mass flow rate (for instance points 1–3 in Fig. 10(a)), an increase in heat flux caused an increase in thermal conductivity and a decrease in viscosity, which led to decreasing Nusselt numbers and increasing Reynolds numbers (points 1–3 in Fig. 10(b)). The result was that the Nusselt numbers and Reynolds numbers accounted for the changes in fluid properties and all the Nusselt numbers of the different heat fluxes (thus different Grashof numbers) collapsed onto a single line. Therefore, for forced convection $Nu \neq g(Gr)$, while $Nu = g(Gr)$ for mixed convection [11]. However, the Nusselt numbers increased with 26% from 4.36 at a Reynolds number of 600 to 5.48 at a Reynolds number of 3064. Therefore, although most textbooks state that $Nu \neq f(Re)$ for laminar forced convection, the experimental data proved that $Nu = f(Re)$ for $Re \geq 1000$. At a Reynolds number of 3064 corresponding to the highest heat flux of 8 kW/m^2, $T_{b,FD}$ was 38.6 °C and the Prandtl number was 4.46. The thermal entrance length was thus 3.49 m (based on $L_t = 0.05 Re Pr D_i$), which confirmed that up to a Reynolds number of 3064, the flow remained fully developed within $680 \leq x/D_i \leq 886$. The increasing Nusselt numbers with Reynolds number were thus not due to developing flow.

The constant forced convection laminar Nusselt number of 4.36 was derived from the velocity and temperature distributions. The velocity distribution was obtained from the momentum equation (Eq. (21)) for fully developed laminar incompressible flow by applying a force balance to a differential volume element [3–7]:

$$\frac{\mu}{r}\frac{d}{dr}\left(r\frac{du}{dr}\right) = \frac{dP}{dx} \tag{21}$$

When assuming μ = constant and dP/dx = constant, Eq. (21) was solved by assuming that the left side of the equation was only a function of r and the right side was only a function of x. For the equality $f(r) = g(x)$ to hold for any value of r and x, they have to be equal to the same constant, therefore dP/dx = constant. The well-known parabolic radial velocity distribution was then obtained by integrating Eq. (21) twice:

$$u(r) = \frac{(D_i/2)^2}{4\mu}\left(\frac{dP}{dx}\right)\left(1 - \frac{r^2}{(D_i/2)^2}\right) \tag{22}$$

Although it was found that both the viscosity and dP/dx were not constant, but decreased along the tube length, the average fluid velocity did not change significantly along the tube length due to the negligible change in density ($\dot{m} = \rho u A$; as the cross-sectional area and mass flow rate remained constant). Furthermore, it is later shown in Fig. 12 that the friction factors corresponded very well to $64/Re$, which confirms that the velocity profile remained parabolic.

The energy equation was obtained by applying an energy balance on a differential volume element, which was then solved to obtain the radial temperature distribution of the fluid:

$$T(r) = T_w - \frac{\dot{q}\left(\frac{D_i}{2}\right)^2}{k}\left(\frac{3}{4} - \frac{r^2}{\left(\frac{D_i}{2}\right)^2} + \frac{r^4}{4\left(\frac{D_i}{2}\right)^4}\right) \tag{23}$$

From the conservation of energy principle, it followed that the energy transported by the fluid through a cross-section must be equal to the energy transported through the same cross section if the fluid was at a constant temperature, T_m. By assuming constant density and specific heat, the mean fluid temperature, T_m, was expressed as:

$$T_m = \frac{2}{V_{avg}(D_i/2)^2}\int_0^{D_i/2} T(r)u(r)rdr \tag{24}$$

By substituting the velocity (Eq. (21)) and temperature (Eq. (23)) profiles into Eq. (24) and combining it with $\dot{q} = h(T_w - T_m)$, a constant Nusselt number of 4.36 (for a constant heat flux boundary condition) that is independent of Reynolds number and Prandtl number, was obtained for a circular tube. It should be noted that this was obtained for constant fluid properties and the variable fluid property results of this study indicated that the Nusselt numbers increased with increasing Reynolds number for Reynolds numbers greater than 1000.

From the friction factor results (Fig. 12) it was concluded that the velocity profile was not significantly affected by the variable fluid properties and remained parabolic, because the friction factors correlated very well with $64/Re$. However, the variable fluid properties significantly affected the temperature profile and thus the thermal boundary layer thickness. Although the flow was fully developed, the mean fluid temperature increased linearly with axial location. This led to a decrease in viscosity and Prandtl number of approximately 13% and 12%, respectively. The Prandtl number represents the ratio of the diffusivity of momentum to the diffusivity of heat. A decreasing Prandtl number therefore indicated that the diffusivity of heat increased along the tube length, which affected the temperature profile and led to a change in Nusselt number.

From Fig. 10 it follows that for Reynolds numbers less than 1000, the change in Nusselt number with Reynolds number was very small and the Nusselt numbers remained approximately constant. This can also be explained with the Prandtl numbers. As the Reynolds numbers were increased, the diffusivity of momentum increased. At low Reynolds numbers, a significant temperature gradient existed along the tube length, therefore a small increase in Reynolds number led to a

significant decrease in temperature and thus increase in Prandtl number. The increase in Prandtl number was mainly due to the increase in momentum diffusivity and not due to the decrease in heat diffusivity. Thus, the temperature profile was not significantly affected, which explains why the Nusselt numbers corresponded well with the constant Nusselt number of 4.36.

A revised fully developed laminar forced convection Nusselt number correlation that accounts for the increase in Nusselt number with Reynolds number, was obtained by a simple power curve fit through all the forced convection heat transfer results for vertical upward and downward flows (Fig. 11(a)):

$$Nu_{FC} = 4.36 + 5.36 \times 10^{-9} Re^{2.39} \quad (25)$$

Eq. (25) is valid for Reynolds numbers between 600 and 3000 (as long as transition does not occur). It should also be noted that the start of transition in horizontal tubes typically occurs in the Reynolds number range of 2100–2300. However, this Reynolds number range is significantly affected by inlet geometry, tube diameter and heat flux [10]. Everts and Meyer [10] found that, for mixed convection conditions, buoyancy effects caused transition to occur earlier (at lower mass flow rates); however, the critical Reynolds numbers increased due to the decreasing viscosity with increasing temperature. Similarly, for forced convection conditions in vertical tubes, increasing heat fluxes significantly increased the critical Reynolds numbers to a Reynolds number range of 2500–3100 (as will be shown in Section 7), due to the decreasing viscosity with increasing temperature. Fig. 11(b) shows the deviation of Eq. (25) from all the upward and downward flow results. From this figure it follows that all the experimental data were within 2.5% of the correlation, and the average deviation was 1.6%. The equation therefore accurately describes the physics of the laminar forced convection Nusselt number dependency on Reynolds number.

6.2. Pressure drop and heat transfer analogy

The laminar fully developed friction factors were compared as a function of Reynolds number for different heat fluxes and flow directions in Fig. 12. Similar to the heat transfer results, this figure indicates that heat flux and flow direction had no influence on the friction factors. The friction factors corresponded very well to the isothermal friction factors of $64/Re$ (solid black line in Fig. 12) with an average and maximum deviation of only 0.9% and 2.8%, respectively. Again, this confirmed that the experimental data presented in this paper is forced convection heat transfer because it was different from the mixed convection conditions where the friction factors were a function of Grashof number [10,11,14,46]. For instance, for horizontal flow [14], mixed convection caused the magnitude of the friction factors to increase by approximately 20% from $64/Re$ at a heat flux of 8 kW/m^2.

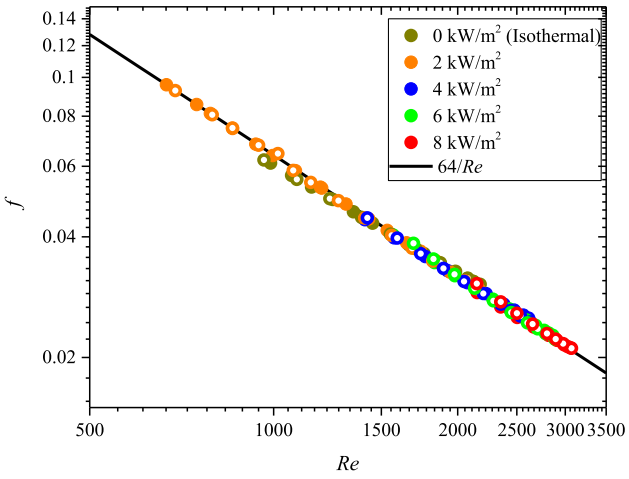

Fig. 12. Comparison of the forced convection diabatic friction factors as a function of Reynolds numbers for vertical upward and downward flow at different heat fluxes.

The relationship between the heat transfer and pressure drop is investigated in Fig. 13 in terms of the ratio of friction factors to the Colburn j-factors, f/j, as a function of Reynolds number for both upward and downward flows. This figure indicates that the f/j-ratio of the different heat fluxes were relatively constant with Reynolds number. The slight differences between the heat fluxes were due to the difference in Prandtl numbers, because the Colburn j-factor was a function of Prandtl number. To account for this, the f/j-ratio was divided by $Pr^{1/3}$ and plotted as a function of Reynolds number in Fig. 13(b). A linear curve fit was done through all the data points and Eq. (26) was obtained as:

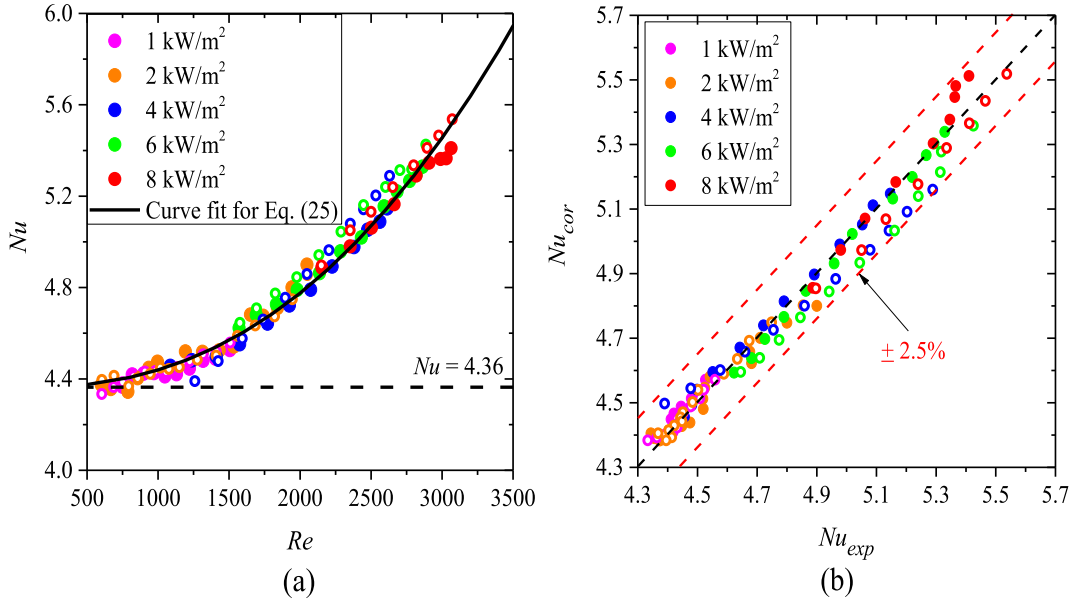

Fig. 11. (a) A linear curve fit through the average laminar forced convection Nusselt numbers as a function of Reynolds number and (b) Comparison of the revised fully developed laminar forced convection Nusselt number correlation (Eq. (25)) with the vertical upward and downward flow experimental data at different heat fluxes.

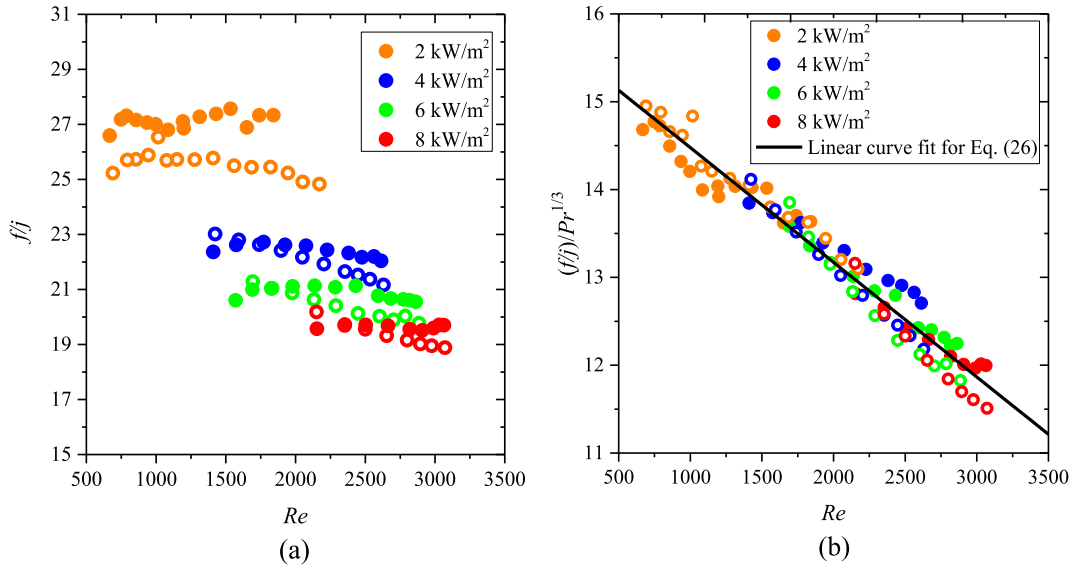

Fig. 13. Comparison of (a) ratio of f/j as a function Reynolds numbers and (b) a linear curve fit through the experimental results for $(f/j)/Pr^{1/3}$ as a function of Reynolds number for both upward and downward flows at different heat fluxes.

$$\frac{(f/j)}{Pr^{\frac{1}{3}}} = 15.78 - 0.0013Re \tag{26}$$

By substituting the Colburn j-factor with Eq. (16), the revised forced convection friction factors were obtained as:

$$f_{FC} = \frac{Nu_{FC}(15.88 - 0.0014Re)}{Re} \tag{27}$$

Because it was known that forced convection conditions existed, the Nusselt numbers was substituted with the revised forced convection Nusselt number (Eq. (25)):

$$f_{FC} = \frac{64}{Re} + \frac{4.8}{Re} - 0.00569 - 7 \times 10^{-12}Re^{2.39} + 8.46 \times 10^{-8}Re^{1.39} \approx \frac{64}{Re} \tag{28}$$

The last two terms of Eq. (28) were negligible because of the small coefficients of 10^{-12} and 10^{-8}. Furthermore, the sum of the second ($4.8/Re$) and third terms (0.00569) was very small and negligible. For example, at a Reynolds number of 1000, the influence of the second and third terms were 1.4%, which was less than the pressure drop uncertainty of 8.5%. Therefore, the maximum contribution of the last four terms in Eq. (28) of all the Reynolds numbers was less than 2.2%.

Eq. (28) therefore reduced to $64/Re$ with a maximum deviation of 2.2%. The experimental data also correlated well with $64/Re$ with a maximum deviation of 2.9%. Therefore, it was concluded that the fluid properties had no significant influence on the forced convection friction factors and were approximately equal to $64/Re$.

7. Results: transitional flow

The heat transfer and pressure drop results were compared at different heat fluxes for vertical upward and downward flows for pure forced convection conditions (as confirmed from the laminar results in Sections 5 and 6). The boundaries of the transitional flow regime in the entrance and fully developed regions were also investigated.

7.1. Heat transfer

Fig. 14 compares the fully developed forced convection Nusselt numbers as a function of Reynolds number for vertical upward and downward flows. This figure indicates that transition occurred at the same critical Reynolds numbers for both upward and downward flow, but was delayed with increasing heat flux. The fact that, for a specific heat flux, transition occurred at the same critical Reynolds number for both upward and downward flow, proved again that the buoyancy effects were negligible, and that pure forced convection existed.

The fact that higher heat fluxes caused transition to occur at a higher Reynolds number was also found in the mixed convection studies by Ghajar and Tam [27] and Everts and Meyer [10]. Although the trends were the same, the specific values of transition were not the same. At the same heat flux, the forced convection critical Reynolds numbers were higher. For example, at a heat flux of 8 kW/m^2 the critical Reynolds number was 3070 for forced convection (vertical flow), while it was 2889 for mixed convection (horizontal flow) [14]. This is as expected because the Grashof numbers of the vertical forced convection cases were higher than for the corresponding horizontal mixed convection cases, and the results of Everts and Meyer [10] showed that the critical Reynolds number increased with increasing Grashof number.

Investigating the raw data of the results in Fig. 14, showed that the delay in transition between the different heat fluxes was primarily because of the changes in the viscosity – transition always occurred at the same mass flow rate for all the heating cases, which corresponded to the mass flow rate of isothermal flow. As explained by Everts and Meyer [10], heating caused the viscosity of the fluid to decrease along the tube

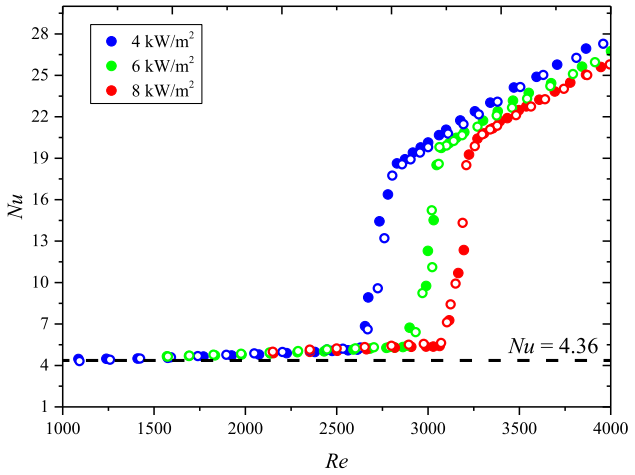

Fig. 14. Average fully developed Nusselt numbers as a function of Reynolds number for vertical upward (●) and downward (○) flows at different heat fluxes.

length, therefore the Reynolds numbers increased. It can therefore be concluded that transition was purely driven by mass flow rate for forced convection heat transfer, while the combined effect of heating and buoyancy affected transition in mixed convection conditions [10,14,27].

The Reynolds numbers at which transition started, Re_{cr}, and ended, Re_{qt}, were plotted for the lowest heat flux of 1 kW/m^2 and the highest heat flux of 8 kW/m^2 in Fig. 15(a). Similar to the results obtained by Everts and Meyer [10,32], the start of transition occurred at the same moment in time along the entire test section, but the local Reynolds numbers increased linearly along the axial location of the tube due to the decreasing viscosity. Furthermore, the gradient of the critical Reynolds numbers increased with increasing heat flux (from 1 to 8 kW/m^2), due to the increased temperature gradient along the tube length [10]. From the solid markers in Fig. 15(a) it follows that the end of the transitional flow regime, Re_{qt}, decreased along the axial location in the entrance region and then increased linearly in the fully developed region. Also, the gradients of the Reynolds numbers at which transition started and ended for each heat flux in the fully developed region were approximately the same.

Fig. 15(b) compares the differences between the Reynolds numbers at which transition started and ended using the width of the transitional flow regime, ΔRe. For all the different heat fluxes (1–8 kW/m^2), the width of the transitional flow regime was a maximum near the inlet of the test section and decreased along the axial location up to the fully developed region where it converged to a constant value of approximately 210. The width of the transitional flow regime became constant at $x/D_i \geq 416$, corresponding to the laminar forced convection thermal entrance length in Fig. 4. From Fig. 15(b) it follows that, for both developing and fully developed flows, heating did not significantly affect the width of the transitional flow regime due, unlike mixed convention in horizontal [10] and inclined [14] tubes, where buoyancy effects decreased the width of transition.

Up to now, only two sets of correlations were available for predicting the start and end of the transitional flow regime for mixed convection in the entrance and fully developed region of smooth tubes. The first set of correlations were developed by Ghajar and Tam [30] and were a function of axial location only. However, as found by Everts and Meyer [10] for mixed convection heat transfer and also shown in Fig. 14 for forced convection heat transfer, heating caused the critical Reynolds numbers to increase.

Everts and Meyer [10] therefore developed the second set of correlations that accounted for both changes in axial position and buoyancy effects (Grashof number). The correlations are valid for forced and mixed convection heat transfer in the entrance and fully developed region. However, for pure forced convection heat transfer, as in this study, the buoyancy forces have negligible or no influence on the boundaries of the transitional flow regime. The mixed convection correlation of Everts and Meyer [10] underpredicted the forced convection transition Reynolds numbers by 11% because it considers the effect of buoyancy on the transition Reynolds numbers.

For pure forced convection heat transfer, the critical Reynolds numbers were divided by the Prandtl number ratio (Pr_b/Pr_w) to account for the effects of heating and plotted as a function axial location in Fig. 16(a).

A linear curve fit was done through all the data points at different heat fluxes for both upward and downward flows to obtain the following correlation to determine the forced convection critical Reynolds number, Re_{cr}:

$$Re_{cr} = \left(1958 + 0.5\frac{x}{D_i}\right)\frac{Pr_b}{Pr_w} \tag{29}$$

Eq. (29) is valid for forced convection heat transfer (independent of Grashof number) and for $1.01 \leq Pr_b/Pr_w \leq 1.25$, $14 \leq x/D_i \leq 886$ and $3.5 \leq Pr \leq 8.1$. As shown by Ghajar and Tam [27] and Bashir et al. [39], the inlet geometry has an effect on transition. This equation is therefore only valid for a square-edged inlet as was used during the experiments for this study. Fig. 16(b) indicates that the average deviation of the correlation (Eq. (29)) from the experimental data was 2.5% and the maximum deviation was 6.6%.

For the end of transition, the Reynolds number, Re_{qt}, was divided by Pr^3, and plotted in Fig. 17(a). A power curve fit was done through all the experimental data of upward and downward flows at different heat fluxes to obtain the following correlation:

$$Re_{qt} = 8770Pr^{-2/3} \tag{30}$$

Eq. (30) is valid for forced convection heat transfer (independent of Grashof number) and for $3.5 \leq Pr \leq 8.1$ and $14 \leq x/D_i \leq 886$. This equation is also valid for a square-edged inlet only. The comparison of Eq. (30) with the experimental data is shown in Fig. 17(b) where the average deviation was 2.3% and the maximum deviation was 9.5%.

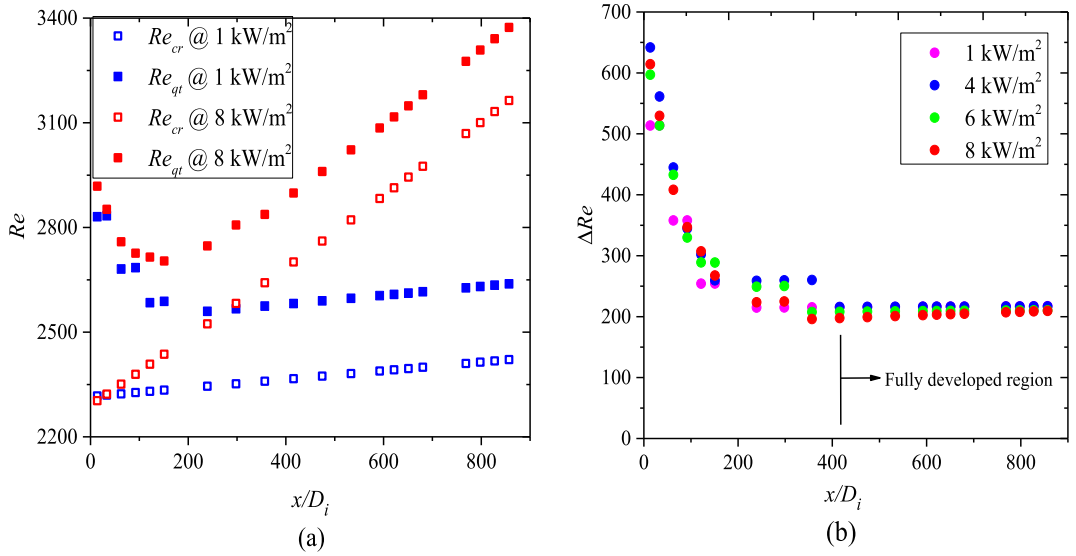

Fig. 15. Comparison for vertical upward flow of (a) Reynolds numbers at which the transitional flow regime started, Re_{cr}, and ended, Re_{qt} and (b) width of the transitional flow regime, ΔRe, as a function axial location for different heat fluxes.

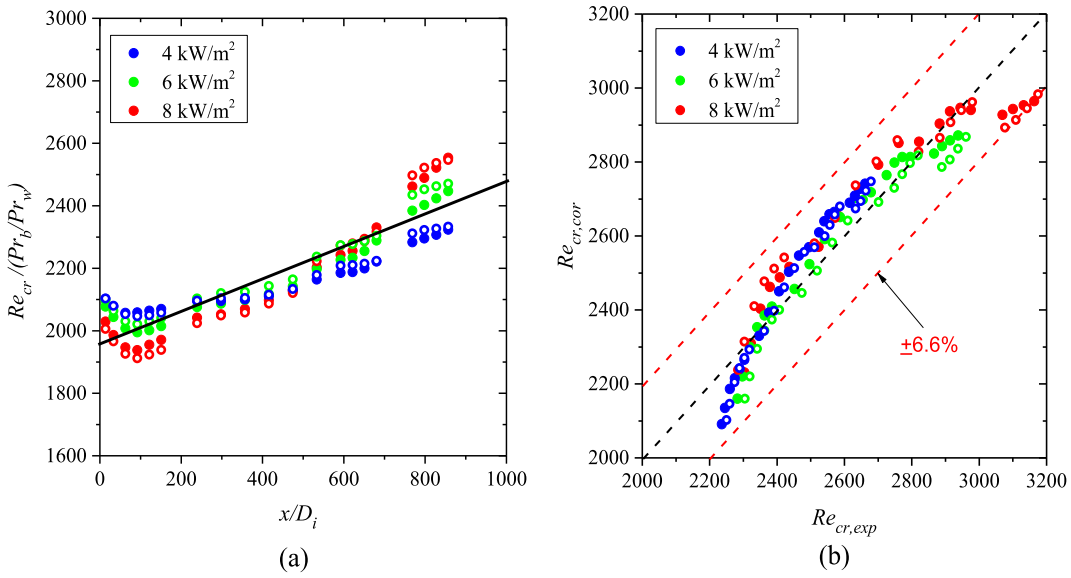

Fig. 16. Comparison of (a) $Re_{cr}/(Pr_b/Pr_w)$ as a function of axial location and (b) the critical Reynolds numbers calculated from Eq. (29) with experimental data for upward and downward flow at different heat fluxes.

7.2. Pressure drop in the transitional flow regime

Fig. 18 shows the forced convection friction factors as a function of bulk Reynolds numbers (Reynolds number at the center of the two pressure taps in Fig. 2) for the heat fluxes of 0 (isothermal), 4, 6, and 8 kW/m^2 for upward and downward flows.

Similar to Fig. 14, transition was independent of flow direction, but was delayed as the heat fluxes increased. The critical Reynolds number at which transition started for isothermal flow was a minimum of 2270 and then increased with increasing heat flux up to a maximum of 3070 at a heat flux of 8 kW/m^2 (Fig. 18). As expected, transition occurred for all the heat fluxes (including isothermal flow) at the same mass flow rate of approximately 0.0081 kg/s and the increasing Reynolds numbers were only due to the decreasing viscosities with increasing temperatures. Similarly, the end of the transitional flow regime Reynolds numbers also increased with increasing heat flux and occurred at approximately the same mass flow rate for the fully developed friction factors.

As the Reynolds numbers at which transition started (Re_{cr}) and ended (Re_{qt}) increased simultaneously with increasing heat flux, the width of the transitional flow regime, ΔRe, remained relatively constant. Again, this is different from mixed convection conditions where the width of the transitional flow regime was significantly affected by the buoyancy effects due to increases in heat flux [10] or inclination angle [14].

Similar to the laminar flow regime, all the friction factors in the quasi-turbulent and turbulent flow regimes were approximately the same for the various heat fluxes in the upward and downward flow configurations.

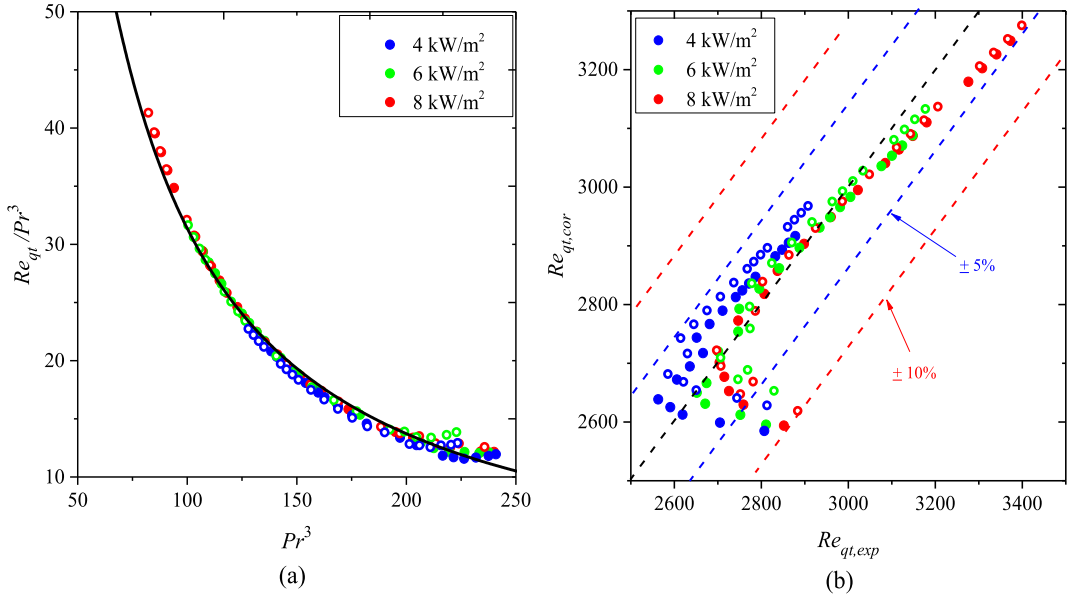

Fig. 17. Comparison of (a) Re_{qt}/Pr^3 as a function of axial location and (b) the Reynolds numbers at which transition ended calculated from Eq. (30) with experimental data in the upward and downward flow directions at different heat fluxes.

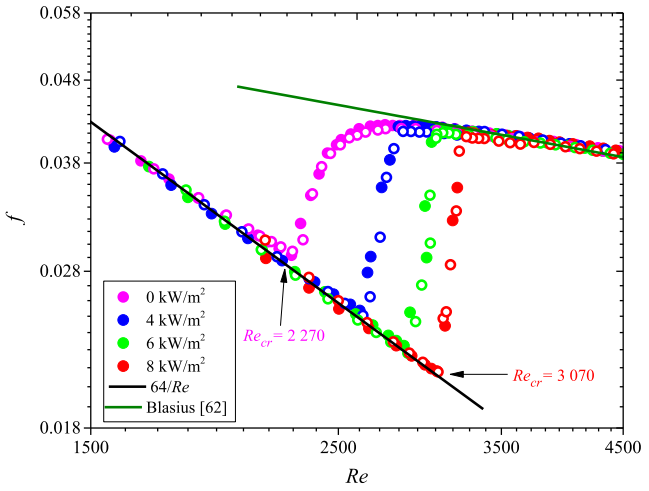

Fig. 18. Comparison of the fully developed friction factors as a function of Reynolds number at different heat fluxes for vertical upward and downward flow. The heat flux of 0 kW/m^{2}was for isothermal flow.

8. Conclusions

Previous experimental literature showed that very limited works were conducted on internal forced convection in the transitional flow regime. Most probably because it is very challenging to perform experiments in the forced convection flow regime. Therefore, the aim of this study was to experimentally investigate the effect of different heat fluxes on the forced convection heat transfer and pressure drop characteristics in the laminar and transitional flow regimes of a smooth circular tube. Experiments were conducted between Reynolds numbers of 400 and 6000 using a copper tube test section, with an inner diameter of 5.1 mm, that was heated at constant heat fluxes from 1 to 8 kW/m^2. To ensure forced convection conditions and negligible buoyancy effects, experiments were conducted with the test section in a vertically upward and downward orientation.

It was found that flow direction had a negligible effect on the Nusselt numbers for Reynolds numbers higher than 600. Furthermore, the fully developed laminar forced convection Nusselt numbers were not constant at 4.36, for a constant heat flux boundary condition, but were a function of Reynolds number, but independent of Grashof number. Heat flux had no influence on the magnitude of the fully developed forced convection friction factors in the laminar flow regime, and the friction factors corresponded well with $f = 64/Re$. A revised laminar fully developed forced convection Nusselt number correlation, which is a function of Reynolds number, was developed for flow in smooth tubes.

The Reynolds numbers at which transition started and ended in the fully developed region increased simultaneously as the heat flux increased for pure forced convection conditions. Furthermore, the width of the transitional flow regime was the same for all heat fluxes and decreased along the length of the tube in the entrance region up to the fully developed region where it remained constant. Correlations were developed to determine the boundaries of the transitional flow regime for pure forced convection. It was concluded from both the heat transfer and pressure drop results that transition occurred at the same mass flow rate for all heat fluxes, which corresponded to the isothermal flow case. However, the Reynolds numbers increased with increasing heat flux due to the decreasing viscosity with increasing temperature.

Declaration of Competing Interest

None.

Acknowledgements

The authors acknowledge the funding received from the Department of Science and Technology (DST) in South Africa and Bayero University Kano in Nigeria. This work was conducted by the first author who is a PhD student under the supervision of the second (post-doctoral fellow) and last (professor) authors. The third author was a visiting professor to the University of Pretoria, during a one-month sabbatical. The sabbatical was part of a project that received funding from the European Union's Horizon 2020 research and innovation programme under the Marie Skłodowska-Curie grant agreement No. 778104.

References

[1] M. Everts, J.P. Meyer, Flow regime maps for smooth horizontal tubes at a constant heat flux, Int. J. Heat Mass Transf. 117 (2018) 1274–1290.
[2] B. Metais, E.R.G. Eckert, Forced, mixed and free convection regimes, ASME J. Heat Transf. 86 (1964) 295–296.
[3] Y.A. Çengel, A.J. Ghajar, Heat and Mass Transfer: Fundamentals & Applications, fifth ed., McGraw Hill, New York, 2015.
[4] J.H. Lienhard, J.H. Lienhard, A Heat Transfer Textbook, fourth ed., Dover Publications, Newburyport, 2013.
[5] A. Bejan, Convection Heat Transfer, fourth ed., J. Wiley & Sons, Hoboken, 2013.
[6] J.P. Holman, Heat Transfer, 10th ed., McGraw-Hill, Boston; London, 2014.
[7] T.L. Bergman, A.S. Lavine, F.P. Incropera, D.P. DeWitt, Fundamentals of Heat and Mass Transfer, 8th ed., Wiley, New York, 2017.
[8] R.K. Shah, A.L. London, Laminar Flow Forced Convection in Duts, Academic Press, New York, 1978.
[9] L.M. Tam, A.J. Ghajar, Effect of inlet geometry and heating on the fully developed friction factor in the transition region of a horizontal tube, Exp. Therm. Fluids Sci. 1777 (97) (1997) 52–64.
[10] M. Everts, J.P. Meyer, Heat transfer of developing and fully developed flow in smooth horizontal tubes in the transitional flow regime, Int. J. Heat Mass Transf. 117 (2018) 1331–1351.
[11] J.P. Meyer, M. Everts, Single-phase mixed convection of developing and fully developed flow in smooth horizontal circular tubes in the laminar and transitional flow regimes, Int. J. Heat Mass Transf. 117 (2018) 1251–1273.
[12] T.M. Hallman, Combined Free and Forced Convection in a Circular Tube, PhD thesis Purdue University, Lafayette, 1958.
[13] Y. Sudo, K. Miyata, H. Ikawa, M. Ohkawara, M. Kaminaga, Experimental study of differences in single-phase forced-convection heat transfer characteristics between upflow and downflow for narrow rectangular channel, J. Nucl. Sci. Technol. 22 (3) (1985) 202–212.
[14] J.P. Meyer, A.I. Bashir, M. Everts, Single-phase mixed convective heat transfer and pressure drop in the laminar and transitional flow regimes in smooth inclined tubes heated at a constant heat flux, Exp. Therm. Fluids Sci. (2019) Manuscript nr: ETF_109890, (accepted on 7 August 2019). https://doi.org/10.1016/j.expthermflusci.2019.109890.
[15] S. Kakaç, The effect of temperature-dependent fluid properties on convective heat transfer, in: S. Kakaç, R.K. Shah, W. Aung (Eds.), Handbook of Single-Phase Convective Heat Transfer, Wiley, New York, 1987.
[16] C. Nonino, S. Del Giudice, S. Savino, Temperature dependent viscosity effects on laminar forced convection in the entrance region of straight ducts, Int. J. Heat Mass Transf. 49 (23) (2006) 4469–4481.
[17] C. Nouar, Numerical solution for laminar mixed convection in a horizontal annular duct: temperature-dependent viscosity effect, Int. J. Numer. Methods Fluids 29 (7) (1999) 849–864.
[18] L. Zhai, G. Xu, Y. Quan, G. Song, B. Dong, H. Wu, Numerical analysis of the axial heat conduction with variable fluid properties in a forced laminar flow tube, Int. J. Heat Mass Transf. 114 (2017) 238–251.
[19] R.G. Deissler, Analytical investigation of fully developed laminar flow in tubes with heat transfer with fluid properties variable along the radius, NACA TN 2410, 1951.
[20] R.L. Shannon, C.A. Depew, Forced laminar flow convection in a horizontal tube with variable viscosity and free-convection effects, J. Heat Transf. 91 (2) (1969) 251–258.
[21] H. Herwig, The effect of variable properties on momentum and heat transfer in a tube with constant heat flux across the wall, Int. J. Heat Mass Transf. 28 (2) (1985) 423–431.
[22] L.B. Koppel, J.M. Smith, Laminar flow heat transfer for variable physical properties, J. Heat Transf. 84 (2) (1962) 157–162.
[23] H. Zhao, X. Li, X. Wu, New friction factor and Nusselt number equations for laminar forced convection of liquid with variable properties, Sci. China Technol. Sci. 61 (1) (2018) 98–109.
[24] H. Herwig, S.P. Mahulikar, Variable property effects in single-phase incompressible flows through microchannels, Int. J. Therm. Sci. 45 (10) (2006) 977–981.
[25] N.P. Gulhane, S.P. Mahulikar, Numerical study of compressible convective heat transfer with variations in all fluid properties, Int. J. Therm. Sci. 49 (5) (2010) 786–796.
[26] R. Kumar, S.P. Mahulikar, Effect of temperature-dependent viscosity variation on fully developed laminar microconvective flow, Int. J. Therm. Sci. 98 (2015) 179–191.

[27] A.J. Ghajar, L.M. Tam, Heat transfer measurements and correlations in the transition region for a circular tube with three different inlet configurations, Exp. Therm. Fluid Sci. 8 (1) (1994) 79–90.
[28] A.J. Ghajar, L.M. Tam, Laminar-transition-turbulent forced and mixed convective heat transfer correlations for pipe flows with different inlet configurations, American Society of Mechanical Engineers, Heat Transfer Division, (Publication) HTD, 1991, pp. 15–23.
[29] L.M. Tam, A.J. Ghajar, Transitional heat transfer in plain horizontal tubes, Heat Transf. Eng. 27 (5) (2006) 23–38.
[30] A.J. Ghajar, L.M. Tam, Flow regime map for a horizontal pipe with uniform wall heat flux and three inlet configurations, Exp. Therm. Fluid Sci. 10 (3) (1995) 287–297.
[31] A.J. Ghajar, L.M. Tam, S.C. Tam, Improved heat transfer correlation in the transition region for a circular tube with three inlet configurations using artificial neural networks, Heat Transf. Eng. 25 (2) (2004) 30–40.
[32] M. Everts, J.P. Meyer, Relationship between pressure drop and heat transfer of developing and fully developed flow in smooth horizontal circular tubes in the laminar, transitional, quasi-turbulent and turbulent flow regimes, Int. J. Heat Mass Transf. 117 (2018) 1231–1250.
[33] J.P. Meyer, M. Everts, A.T.C. Hall, F.A. Mulock-Houwer, M. Joubert, L.M.J. Pallent, E.S. Vause, Inlet tube spacing and protrusion inlet effects on multiple circular tubes in the laminar, transitional and turbulent flow regimes, Int. J. Heat Mass Transf. 118 (2018) 257–274.
[34] J.P. Meyer, S.M. Abolarin, Heat transfer and pressure drop in the transitional flow regime for a smooth circular tube with twisted tape inserts and a square-edged inlet, Int. J. Heat Mass Transf. 117 (2018) 11–29.
[35] S.M. Abolarin, M. Everts, J.P. Meyer, The influence of peripheral u-cut twisted tapes and ring inserts on the heat transfer and pressure drop characteristics in the transitional flow regime, Int. J. Heat Mass Transf. 132 (2019) 970–984.
[36] S.M. Abolarin, M. Everts, J.P. Meyer, Heat transfer and pressure drop characteristics of alternating clockwise and counter clockwise twisted tape inserts in the transitional flow regime, Int. J. Heat Mass Transf. 133 (2019) 203–217.
[37] T. Wei, Heat transfer regimes in fully developed plane-channel flows, Int. J. Heat Mass Transf. 131 (2019) 140–149.
[38] D. Huber, H. Walter, Forced convection heat transfer in the transition region between laminar and turbulent flow for a vertical circular tube, in: Proceedings of the 2010 International Conference on Theoretical and Applied Mechanics, and 2010 International Conference on Fluid Mechanics and Heat & Mass Transfer, World Scientific and Engineering Academy and Society (WSEAS), Corfu Island, Greece, 2010, pp. 132–136.
[39] A.I. Bashir, M. Everts, J.P. Meyer, Influence of inlet contraction ratios on the heat transfer and pressure drop characteristics of single-phase flow in smooth circular tubes in the transitional flow regime, Exp. Therm. Fluids Sci. (2019) Manuscript nr: ETF_109892, (accepted on 7 August 2019). https://doi.org/10.1016/j.expthermflusci.2019.109892.
[40] N. Galanis, A. Behzadmehr, Mixed convection in vertical ducts, in: International Conference on Fluid Mechanics and Aerodynamics (FMA'08), Rhodes, Greece, 2008, pp. 6–12.
[41] G.F. Scheele, E.M. Rosen, T.J. Hanratty, Effect of natural convection on transition to turbulence in vertical pipes, Canad. J. Chem. Eng. 38 (3) (1960) 67–73.
[42] A. Behzadmehr, A. Laneville, N. Galanis, Experimental study of onset of laminar – turbulent transition in mixed convection in a vertical heated tube, Int. J. Heat Mass Transf. 51 (25–26) (2008) 5895–5905.
[43] M. Everts, Heat Transfer and Pressure Drop of Developing Flow in Smooth Tubes in the Transitional Flow Regime, Masters Dissertation, University of Pretoria, Pretoria, 2014.
[44] A. Bakker, R.D. LaRoche, E.M. Marshall, Laminar flow in static mixers with helical elements, The Online CFM Book (2000).
[45] M. Everts, Single-phase Mixed Convection of Developing and Fully Developed Flow in Smooth Horizontal Circular Tubes in the Laminar, Transitional, Quasi-turbulent and Turbulent Flow Regimes, PhD thesis University of Pretoria, Pretoria, 2018.
[46] K.H. Tam, L.M. Tam, A.J. Ghajar, Effect of inlet geometries and heating on the entrance and fully-developed friction factors in the laminar and transition regions of a horizontal tube, Exp. Therm. Fluid Sci. 44 (2013) 680–696.
[47] R.E. Rayle, Influence of orifice geometry on static pressure measurements, ASME paper No 59-A-234, 1959.
[48] G.P. Celata, D.A. Francesco, C. Andrea, M. Cumo, Upflow turbulent mixed convection heat transfer in vertical pipes, Int. J. Heat Mass Transf. 41 (1998) 3926–3943.
[49] H.A. Mohammed, Laminar mixed convection heat transfer in a vertical circular tube under buoyancy-assisted and opposed flows, Energy Conver. Manage. 49 (2008) 2006–2015.
[50] D.D. Joye, Comparison of correlations and experiment in opposing flow, mixed convection heat transfer in a vertical tube with Grashof number variation, Int. J. Heat Mass Transf. 39 (5) (1996) 1033–1038.
[51] P.E. Saylor, D.D. Joye, Hydrostatic correction and pressure drop measurement in mixed convection heat transfer in a vertical tube, Industr. Eng. Chem. Res. 30 (4) (1991) 784–788.
[52] T. Maré, N. Galanis, I. Voicu, J. Miriel, Experimental analysis of mixed convection in inclined tubes, Appl. Therm. Eng. 26 (14–15) (2006) 1677–1683.
[53] C.O. Popiel, J. Wojtkowiak, Simple formulas for thermophysical properties of liquid water for heat transfer calculations (from 0 °C to 150 °C), Heat Transf. Eng. 19 (3) (1998) 87–101.
[54] C. Wang, P. Gao, S. Tan, Z. Wang, C. Xu, Experimental study of friction and heat transfer characteristics in narrow rectangular channel, Nucl. Eng. Des. 250 (2012) 646–655.
[55] C. Wang, P. Gao, S. Tan, Z. Wang, Forced convection heat transfer and flow characteristics in laminar to turbulent transition region in rectangular channel, Exp. Therm. Fluid Sci. 44 (2013) 490–497.
[56] J. Ma, L. Li, Y. Huang, X. Liu, Experimental studies on single-phase flow and heat transfer in a narrow rectangular channel, Nucl. Eng. Des. 241 (8) (2011) 2865–2873.
[57] T.S. Zhao, Q.C. Bi, Pressure drop characteristics of gas–liquid two-phase flow in vertical miniature triangular channels, Int. J. Heat Mass Transf. 44 (13) (2001) 2523–2534.
[58] F. Madrid, N. Caney, P. Marty, Study of a vertical boiling flow in rectangular mini-channels, Heat Transf. Eng. 28 (8–9) (2007) 753–760.
[59] M.V. Sardeshpande, P. Shastri, V.V. Ranade, Two-phase flow boiling pressure drop in small channels, Int. J. Heat Fluid Flow 61 (2016) 636–649.
[60] P.F. Dunn, Measurement and Data Analysis for Engineering and Science, second ed., CRC Press, United States of America, 2010.
[61] J.L. Poiseuille, Recherches expérimentales sur le mouvement des liquides dans les tubes de très- petits diamètres, Imprimerie Royale (1844).
[62] H. Blasius, Das ähnlichkeitsgesetz bei reibungsvorgangen in flüssigkeiten, Forschg Arb. Ing.-Wes (1913) 131–137.
[63] B. Metais, E.R.G. Eckert, Forced, mixed, and free convection regimes, J. Heat Transf. 86 (2) (1964) 295–296.
[64] V. Gnielinski, New equations for heat and mass-transfer in turbulent pipe and channel flow, Int. Chem. Eng. 16 (2) (1976) 359–368.
[65] J.P. Meyer, M. Everts, N. Coetzee, K. Grote, M. Steyn, Heat transfer coefficients of laminar, transitional, quasi-turbulent and turbulent flow in circular tubes, Int. Commun. Heat Mass Transf. 105 (2019) 84–106.
[66] C.J. Ho, C.Y. Chang, C.Y. Cheng, S.J. Cheng, Y.W. Guo, S.T. Hsu, W.M. Yan, Laminar forced convection effectiveness of Al2O3–water nanofluid flow in a circular tube at various operation temperatures: effects of temperature-dependent properties, Int. J. Heat Mass Transf. 100 (2016) 464–481.